A Compound with a New Type of Butterfly Metal Atom Cluster: $[N(C_4H_9)_4]_2[Mo_4OBr_{12}]$

F. Albert Cotton,* Xuejun Feng, Maoyu Shang, and Zhong Sheng Sun

Department of Chemistry and Laboratory for Molecular Structure and Bonding, Texas A&M University, College Station, Texas 77843

Received September 11, 1992

The reaction of molybdenum(III) bromide with a mixture of acetic acid and acetic anhydride in the presence of $[N(C_4H_9)_4][BF_4]$ affords the title compound. It was isolated as a crystalline solvate containing $0.5(CH_3)_2CO$ and the structure determined. The anion has a butterfly array of molybdenum atoms with an internal dihedral angle of 118.6°. The Mo–Mo distances around the periphery have an average value of 2.671[3] Å while that between hinge atoms is 2.594(1) Å. There is a μ_4-O atom making distances of 2.061[9] Å to the wingtip Mo atoms and 2.104[3] Å to the hinge Mo atoms, with Mo–O–Mo angles of 153.9(3) and 76.1(2)°, respectively. The structure can be regarded as a fragment of a $Mo_6(\mu_3\text{-}Br)_8Br_6$ octahedral cluster from which two adjacent Mo–Br units have been deleted, followed by insertion of the μ_4-O atom. Alternatively, it may be regarded as two triangle $Mo_3(\mu_3\text{-}O)(\mu_3\text{-}Br)(\mu_2\text{-}Br)_3Br_6$ clusters fused on a common Mo–Mo–O face. The crystallographic parameters are as follows: space group $P\bar{1}$, $a = 12.755(2)$ Å, $b = 21.192(3)$ Å, $c = 11.692(2)$ Å, $\alpha = 103.53(1)°$, $\beta = 107.99(1)°$, $\gamma = 82.00(1)°$, $V = 2914.6(7)$ Å^3, $Z = 2$. By using 6714 observed reflections, 472 parameters were refined to $R = 0.054$, $R_w = 0.087$. Molecular orbital calculations (Fenske–Hall and SCF–Xα–SW) have been carried out for $[Mo_4OX_{12}]^{2-}$, $[Mo_4Cl_{12}]^{3-}$, and Mo_4Cl_{12} clusters, and the results have been analyzed on the basis of the clusters in molecules concept. It is found that a set of five strong Mo–Mo bonds exists with additional structural support by interaction of the oxygen 2p orbitals with all of the molybdenum atoms.

Introduction

The chemistry of the "high-valence" or "lower halide" type of metal atom cluster compounds[1-3] has, in recent years, moved in an interesting new direction. While the longest known members of this class are the octahedral M_6 species, such as $[Nb_6Cl_{18}]^{4-}$ and $[Mo_6Cl_{14}]^{2-}$, recent work has turned up smaller clusters, M_5, M_4, and M_3, which have been described as fragments of the octahedron.[4-10] Although, as has been pointed out,[10] this concept of an incomplete octahedron has little if any value in understanding the chemical properties of the compound, it is embedded in the current literature, and it is perhaps of use as a structure-visualizing device and a mnemonic.

One of the largest groups of "octahedral fragments" are the M_4 butterfly structures, which are envisioned as octahedra lacking two adjacent vertices. Three types have previously been described: $[Mo_4I_{11}]^{2-}$ (I), which has an atom (I) bridging the wingtips and a cluster electron population of 15; $[Mo_4Cl_{12}]^{3-}$ (II), in which each wingtip atom has its own additional ligand atom but the electron count is still 15; Mo_4Br_4 (O-*i*-Pr)$_8$ (III), which is structurally like $[Mo_4Cl_{12}]^{3-}$ but has only 12 cluster electrons. A theoretical analysis[9] has provided an account of the bonding in III but left the electronic structures of I and II unaccounted for. It may be noted that the structural difference between I and II may not necessarily have any major consequences for the electronic structure of the cluster, since it is merely a question of replacing A by B:

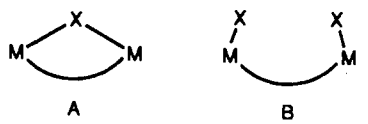

We report here the preparation and structure of a new butterfly cluster of molybdenum in which the number of ligand atoms (13) is greater than any previous number (11 or 12) and the cluster electron count is 12. We also provide a more comprehensive examination of the electronic structures of the various types of butterfly species, i.e., I–III and the new one reported here.

Experimental Section

General Procedures. As a precautionary measure because of possible instability of intermediates, all preparations were carried out under an atmosphere of argon unless otherwise specified. Standard Schlenk and vacuum line techniques were used. $MoBr_3 \cdot 3H_2O$ was prepared according to the literature method.[11] The other chemicals were purchased from commercial sources.

Preparation of $[Bu_4N]_2[Mo_4OBr_{12}]\cdot{}^1/_2Me_2CO$ (1). Molybdenum tribromide trihydrate (4.00 g, 10.3 mmol) and tetrabutylammonium tetrafluoroborate (1.69 g, 5.13 mmol) were stirred with an excess of acetic acid (40 mL) and acetic anhydride (10 mL) at 80 °C for 1 day. This resulted in a mixture of a red-purple solution and a brown precipitate, which were separated by filtration. The brown precipitate was treated with 20 mL of acetone to form a brown solution, which was then filtered and layered with hexane. Two types of crystals were formed after the diffusion process was complete. X-ray diffraction analyses showed that the brown crystals have the formula $[Bu_4N]_2[Mo_4OBr_{12}]\cdot{}^1/_2Me_2CO$ and the green-brown ones have the formula $[Bu_4N]_2[Mo_3OBr_6(OAc)_3]\cdot Me_2CO$. Yields: ca. 20% for $[Bu_4N]_2[Mo_4OBr_{12}]\cdot{}^1/_2Me_2CO$ and ca. 10% for $[Bu_4N]_2[Mo_3OBr_6(OAc)_3]\cdot Me_2CO$. Anal. Calc for $[Bu_4N]_2[Mo_4OBr_{12}]\cdot{}^1/_2Me_2CO$: C, 21.48; H, 4.04; N, 1.50. Found: C, 21.98; H, 3.85; N, 1.84.

(1) These terms are both used[2,3] to distinguish between those clusters in which the metal atoms have oxidation states of +2 or +3 and halide or oxide ligands and the so-called "low-valence" or "carbonyl" type where oxidation numbers are ca. 0 and the ligands are mainly CO, η^5-C_5H_5 and the like.

(2) Cotton, F. A.; Wilkinson, G. *Advanced Inorganic Chemistry*, 5th ed.; John Wiley and Sons: New York, 1988; pp 1052–1054.
(3) Cotton, F. A. *ACS Symp. Ser.* **1983**, *211*, 209.
(4) Jodden, R.; von Schnering, H. G.; Schafer, H. *Angew. Chem.* **1975**, *87*, 595.
(5) (a) Schafer, H.; von Schnering, H. G. *Angew. Chem.* **1971**, *83*, 75. (b) Glicksman, H. D.; Walton, R. A. *Inorg. Chem.* **1978**, *17*, 3197.
(6) Chisholm, M. H.; Errington, R. S.; Folting, K.; Huffman, J. C. *J. Am. Chem. Soc.* **1982**, *104*, 2025.
(7) Aufdembrik, B. A.; McCarley, R. E. *J. Am. Chem. Soc.* **1986**, *108*, 2474.
(8) Chisholm, M. H.; Clark, D. L.; Errington, R. J.; Folting, K.; Huffman, J. C. *Inorg. Chem.* **1988**, *27*, 2071.
(9) Bursten, B. E.; Chisholm, M. H.; Clark, D. L. *Inorg. Chem.* **1988**, *27*, 2084.
(10) Cotton, F. A.; Poli, R. *J. Am. Chem. Soc.* **1988**, *110*, 830.
(11) Brauer, G. *Handbook of Preparative Inorganic Chemistry*; 1965; p 1408.

0020-1669/93/1332-1321$04.00/0

Table I. Crystallographic Data and Data Collection Parameters for $[Bu_4N]_2[Mo_4OBr_{12}]\cdot{}^1/_2Me_2CO$

chem formula	$Mo_4Br_{12}O_{1.5}N_2C_{33.5}H_{75}$	γ, deg	82.00(1)
		Z	2
fw	1872.65	T, °C	23 ± 2
space group (No.)	$P\bar{1}$ (2)	λ, Å	1.541 84
		ρ_{calcd}, g cm^{-3}	2.134
a, Å	12.755(2)	μ(Mo Kα), cm^{-1}	170.33
b, Å	21.192(3)	data collcn instrument	Rigaku AFC5R
c, Å	11.692(2)	transm coeff	100.00–61.68
α, deg	103.53(1)	$R(F_o)$,[a] $R_w(F_o)$[b]	0.054, 0.087
β, deg	107.99(1)		

[a] $R = \sum||F_o| - |F_c||/\sum|F_o|$. [b] $R_w = [\sum w(|F_o| - |F_c|)^2/\sum w|F_o|^2]^{1/2}$; $w = 1/\sigma^2(|F_o|)$.

The purple filtrate was evaporated to dryness and the resulting solid was dissolved in acetone to give a purple solution, which was filtered and then layered with hexane. Dark purple crystals were formed after standing for several days. They were characterized by X-ray crystallographic analysis as $[Bu_4N][Mo_3OBr_6(OAc)_3]\cdot Me_2CO$. Yield: ca. 50%.

Magnetic Measurements. The magnetic susceptibility was measured on a SQUID magnetometer from 50 to 340 K in the laboratory of Professor Timir Datta, Department of Physics, University of South Carolina. The measured results are available as supplementary material.

X-ray Crystallography. A fragment of a brown crystal was mounted on the top of a thin glass fiber with epoxy cement. The intensity data of the compound were collected on a Rigaku AFC5R automatic four-circle diffractometer with Cu Kα radiation (λ = 1.540 598 Å) as the incident beam. Unit cell dimensions were determined by accurately centering 25 reflections. Axial photographs were taken to confirm the Laue class, symmetry, axial lengths, and quality of the crystal. Data reduction and corrections were conducted by the standard methods used in this laboratory.[12,13] Three standard reflections were monitored throughout data collection to check crystal decay and orientation change. An empirical absorption correction was applied based on the ψ scan data of seven reflections with their χ angles near 90°.

No systematic absences were observed. Two space groups $P1$ and $P\bar{1}$ could be assigned to the crystal. We arbitrarily assumed that the space group was $P\bar{1}$, and this was fully confirmed by successful refinement of the structure. Positions of four independent molybdenum atoms were derived by the direct methods (SHELXS-86). The other atoms were then located and refined by alternating difference Fourier syntheses and least-squares refinements. The interstitial acetone molecule was found to be disordered around an inversion center (0.5, 1.0, 0.5) in such a manner that the two terminal carbon atoms were located on positions that were related by the inversion center, and the central carbon atom and the oxygen atom were disordered on two sets of positions that were related by the inversion center. In the last cycle of refinement all non-hydrogen atoms of the cations and anion were refined anisotropically, and the atoms of the interstitial acetone molecule were refined isotropically with final residuals $R = 0.054$ and $R_w = 0.087$ for the fit of 472 variables to 6714 data with $F_o^2 \geq 3\sigma(F_o^2)$. The highest residual electron density in the final difference Fourier map was 1.66. This and a few other residual peaks were found around the metal atoms. Tables I and II list crystallographic data and positional and equivalent isotropic thermal parameters for $[Bu_4N]_2[Mo_4OBr_{12}]\cdot{}^1/_2Me_2CO$.

Computational Procedures. Molecular orbital calculations were performed for a model butterfly cluster compound $[Mo_4(\mu_4\text{-}O)(\mu_3\text{-}Cl)_2(\mu_2\text{-}Cl)_4Cl_6]^{2-}$ by using both the Fenske–Hall method[14a] and the SCF–Xα–SW method.[15a] To facilitate analysis of molecular bonding, two fragments of the model compound, $[Mo_4]^{12+}$ and $[Mo_4O]^{10+}$, were also calculated by the Fenske–Hall method. In addition, for the purpose of comparison, the calculations were also carried out for a model compound, $Mo_4(\mu_3\text{-}Cl)_2(\mu_2\text{-}Cl)_4Cl_6$, and two actual compounds, namely, $[Mo_4(\mu_4\text{-}O)(\mu_3\text{-}Br)_2(\mu_2\text{-}Br)_4Br_6]^{2-}$ and $[Mo_4(\mu_3\text{-}Cl)_2(\mu_2\text{-}Cl)_4Cl_6]^{3-}$.[7] The basis functions employed in the Fenske–Hall calculations were obtained by fitting numerical Xα atomic orbitals to analytical Slater type orbitals.[14b] For the SCF–Xα–SW calculations, Schwarz's α atomic exchange parameters[15b] were used with a valence electron weighted average of the atomic α values for the inter- and outer-sphere regions in each calculation. Overlapping atomic sphere radii were taken as 89% of the atomic number radii calculated by the molecular superposition program.[15c]

The atomic coordinates for the model cluster $[Mo_4OCl_{12}]^{2-}$ were determined mainly from the crystal structure[7] of $[Mo_4Cl_{12}]^{3-}$, and were idealized to C_{2v} symmetry. The Mo–Mo distances used were 2.60 Å between the hinge molybdenum atoms (Mo_h) and 2.55 Å between the hinge and wingtip molybdenum atoms (Mo_w). The metal to μ_3-Cl (Cl_c), μ_2-Cl (Cl_b) and terminal Cl (Cl_t) distances used were 2.50, 2.44, and 2.47 Å, respectively. The dihedral angle between the two Mo_3 planes were assumed to be 120°. The coordinates of the oxygen atom were obtained with the distances of the oxygen to the hinge and wingtip molybdenum

Table II. Positional and Equivalent Isotropic Thermal Parameters for Non-Hydrogen Atoms of $[Bu_4N]_2[Mo_4OBr_{12}]\cdot{}^1/_2Me_2CO$

atom	x	y	z	B,[a] Å^2
Mo(1)	0.32965(6)	0.73962(4)	0.13876(7)	2.47(2)
Mo(2)	0.20031(6)	0.66924(3)	0.18110(6)	2.33(2)
Mo(3)	0.39888(6)	0.68926(4)	0.34162(7)	2.51(2)
Mo(4)	0.13520(6)	0.79332(4)	0.16753(6)	2.27(2)
Br(1)	0.37799(9)	0.61510(5)	0.1233(1)	4.09(3)
Br(2)	0.14493(9)	0.70659(5)	–0.02841(9)	4.02(2)
Br(3)	0.51640(9)	0.76394(6)	0.2955(1)	4.97(3)
Br(4)	0.27467(9)	0.86025(5)	0.1382(1)	4.14(2)
Br(5)	0.26092(9)	0.62482(5)	0.37935(9)	4.13(2)
Br(6)	0.01844(8)	0.72154(6)	0.2215(1)	4.45(3)
Br(7)	0.4153(1)	0.73598(7)	–0.0330(1)	5.81(3)
Br(8)	0.1059(1)	0.56519(5)	0.0710(1)	5.27(3)
Br(9)	0.4249(1)	0.75758(6)	0.5538(1)	4.75(3)
Br(10)	0.5599(1)	0.61289(6)	0.4218(1)	5.59(3)
Br(11)	0.1173(1)	0.88014(5)	0.34979(9)	4.34(3)
Br(12)	–0.0305(1)	0.84746(6)	0.0313(1)	5.31(3)
O(1)	0.2685(5)	0.7555(3)	0.2918(5)	2.6(1)
N(1)	0.2671(7)	0.3709(4)	0.1808(8)	4.0(2)
C(1)	0.229(1)	0.3043(6)	0.174(1)	6.0(4)
C(2)	0.251(1)	0.2881(6)	0.304(1)	7.3(4)
C(3)	0.201(1)	0.2267(7)	0.299(2)	8.9(5)
C(4)	0.223(2)	0.2144(8)	0.428(2)	9.0(5)
C(5)	0.226(1)	0.3844(8)	0.053(1)	6.0(4)
C(6)	0.264(1)	0.3394(9)	–0.049(1)	8.2(5)
C(7)	0.232(1)	0.364(1)	–0.165(2)	10.4(5)
C(8)	0.298(2)	0.410(1)	–0.158(2)	17.8(9)
C(9)	0.2226(9)	0.4263(6)	0.268(1)	4.8(3)
C(10)	0.100(1)	0.4308(7)	0.251(1)	6.1(4)
C(11)	0.062(1)	0.4856(9)	0.333(2)	7.8(4)
C(12)	–0.056(2)	0.493(1)	0.325(2)	10.9(7)
C(13)	0.393(1)	0.3650(8)	0.229(1)	7.1(4)
C(14)	0.447(1)	0.424(1)	0.219(2)	9.1(5)
C(15)	0.576(1)	0.414(1)	0.302(2)	10.7(7)
C(16)	0.647(2)	0.444(1)	0.264(2)	12.5(8)
N(2)	0.1796(7)	0.9253(4)	0.7559(7)	3.6(2)
C(17)	0.0895(9)	0.9460(5)	0.822(1)	4.4(3)
C(18)	–0.023(1)	0.9470(6)	0.738(1)	4.9(3)
C(19)	–0.103(1)	0.9724(7)	0.813(1)	6.3(4)
C(20)	–0.221(1)	0.9706(7)	0.738(2)	8.0(5)
C(21)	0.2885(9)	0.9202(6)	0.8573(9)	4.2(3)
C(22)	0.394(1)	0.8998(7)	0.817(1)	5.7(3)
C(23)	0.496(1)	0.9001(7)	0.927(1)	6.5(4)
C(24)	0.601(2)	0.873(1)	0.885(2)	11.3(7)
C(25)	0.185(1)	0.9754(6)	0.683(1)	5.2(3)
C(26)	0.213(1)	1.0419(5)	0.755(1)	5.0(3)
C(27)	0.211(1)	1.0872(7)	0.670(1)	7.0(4)
C(28)	0.241(2)	1.1559(7)	0.740(2)	9.4(5)
C(29)	0.158(1)	0.8623(6)	0.666(1)	4.9(3)
C(30)	0.148(1)	0.8045(6)	0.714(1)	4.9(3)
C(31)	0.113(1)	0.7482(8)	0.598(2)	8.3(4)
C(32)	0.103(1)	0.6865(8)	0.631(1)	7.8(4)
O(2)	0.544(3)	0.986(2)	0.347(3)	13(1)*
C(33)	0.476(2)	0.938(1)	0.474(2)	11.4(7)*
C(34)	0.527(4)	1.002(3)	0.450(4)	12(1)*

[a] Anisotropically refined atoms are given in the form of the equivalent isotropic displacement parameter defined as $^1/_3[a^2a^{*2}B_{11} + b^2b^{*2}B_{22} + c^2c^{*2}B_{33} + 2ab(\cos\gamma)a^*b^*B_{12} + 2ac(\cos\beta)a^*c^*B_{13} + 2bc(\cos\alpha)b^*c^*B_{23}]$. Starred values indicate atoms were refined isotropically.

(12) (a) Bino, A.; Cotton, F. A.; Fanwick, P. E. *Inorg. Chem.* **1979**, *18*, 3558. (b) Cotton, F. A.; Frenz, B. A.; Deganello, G.; Shaver, A. *J. Organomet. Chem.* **1973**, *50*, 227.

(13) Crystallographic computing was done on a local area VAX cluster, employing the VAX/VMS V4.6 computer and Enraf-Nonius SDP software.

(14) (a) Hall, M. B.; Fenske, R. F. *Inorg. Chem.* **1972**, *11*, 768. (b) Sargent, A. L.; Hall, M. B. *Polyhedron* **1990**, *9*, 1799.

(15) (a) Slater, J. C. *Quantum Theory of Molecules and Solids*; McGraw-Hill: New York, 1974; Vol. 4. (b) Schwarz, K. *Phys. Rev. B* **1972**, *5*, 2466. (c) Norman, J. G., Jr. *Mol. Phys.* **1976**, *31*, 1191.

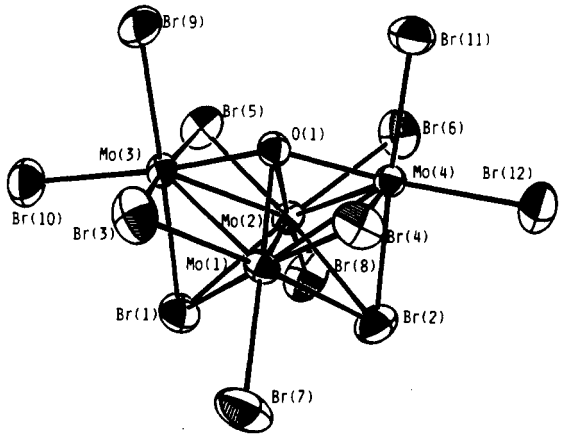

Figure 1. ORTEP drawing of the $[Mo_4OBr_{12}]^{2-}$ ion. Each atom is represented by its ellipsoid of thermal displacement at the 50% probability level, and the numbering used in the tables is defined.

atoms taken as 2.104 and 2.000 Å, respectively. The structural parameters used in the calculation of the model compound, Mo_4Cl_{12}, were the same as those for $[Mo_4Cl_{12}]^{3-}$. The coordinates of the atoms in each fragment calculated were the same as they were in the whole system.

Results and Discussion

Structure. The structure of the anion is shown in Figure 1, and the principal bond distances and angles are listed in Table III. The four molybdenum atoms have a butterfly arrangement with a hinge angle (the dihedral angle between the two Mo_3 planes) of 118.6°. There is a capping bromine atom below each external triangular face and a bridging bromine atom on each edge except the hinge edge. In addition there is one terminal bromine atom on each hinge Mo atom and two on each wingtip Mo atom. Finally there is an oxygen atom nestled into the Mo_4 cluster. It lies on a perpendicular bisector of the hinge and just above a line between the wingtip Mo atoms. While there is no crystallographically required symmetry, the $[Mo_4OBr_{12}]^{2-}$ ion has effectively C_{2v} symmetry.

The four peripheral (i.e., hinge-to-wingtip) Mo–Mo bonds are in the range 2.666(1)–2.678(1) Å, with a mean value of 2.671[3] Å, and the hinge Mo–Mo bond length is 2.594(1) Å. The μ_3-O atom is located at mean distances of 2.061[9] and 2.104[3] Å from the wingtip and hinge molybdenum atoms, respectively.

The structure of the $[Mo_4OBr_{12}]^{2-}$ ion can be regarded as formed by two bicapped Mo_3 clusters of the type $Mo_3(\mu_3\text{-}Br)(\mu_3\text{-}O)(\mu_2\text{-}Br)_3Br_6$ fused together so as to share the oxygen atom, two Mo atoms and some of the bromine atoms. The deviations of each local Mo_3OBr_{10} unit from C_{3v} symmetry are quite small, the largest being less than 0.1 Å.

Electronic Structure Calculations. The results obtained by the Fenske–Hall molecular orbital method for the butterfly cluster $[Mo_4OCl_{12}]^{2-}$ are very similar to those obtained by the Xα–SW method. Although the latter is more rigorous, it is much less convenient both to carry out and to interpret in orbital terms. We shall, therefore, consider the electronic structure and bonding in $[Mo_4OCl_{12}]^{2-}$ mainly on the basis of results given by the Fenske–Hall molecular orbital calculations. Furthermore, the results will be presented in terms of the idea[9,16] of "clusters in molecules", by transforming the molecular orbitals of the whole molecule or a fragment into a basis consisting of the canonical orbitals of the bare metal cluster $[Mo_4]^{12+}$ and the atomic orbitals of the relevent ligands. This approach, implemented by the use of the Fenske–Hall MO calculations, has already been shown to be very effective in understanding the bonding in metal cluster compounds.[9,16]

(16) (a) Bursten, B. E.; Cotton, F. A.; Hall, M. B.; Najjar, R. C. *Inorg. Chem.* **1982**, *21*, 302. (b) Cotton, F. A.; Diebold, M. P.; Feng, X.; Roth, W. J. *Inorg. Chem.* **1988**, *27*, 3413.

Table III. Selected Bond Lengths (Å) and Angles (deg) for $[Bu_4N]_2[Mo_4OBr_{12}]\cdot{}^1/_2Me_2CO$[a]

Distances

Mo(1)–Mo(2)	2.594(1)	Mo(2)–Br(8)	2.534(1)
Mo(1)–Mo(3)	2.678(1)	Mo(2)–O(1)	2.101(5)
Mo(1)–Mo(4)	2.667(1)	Mo(3)–Br(1)	2.622(1)
Mo(1)–Br(1)	2.602(1)	Mo(3)–Br(3)	2.569(2)
Mo(1)–Br(2)	2.615(1)	Mo(3)–Br(5)	2.566(2)
Mo(1)–Br(3)	2.550(1)	Mo(3)–Br(9)	2.511(1)
Mo(1)–Br(4)	2.556(1)	Mo(3)–Br(10)	2.512(1)
Mo(1)–Br(7)	2.547(2)	Mo(3)–O(1)	2.052(5)
Mo(1)–O(1)	2.106(7)	Mo(4)–Br(2)	2.605(1)
Mo(2)–Mo(3)	2.6660(9)	Mo(4)–Br(4)	2.569(2)
Mo(2)–Mo(4)	2.671(1)	Mo(4)–Br(6)	2.567(2)
Mo(2)–Br(1)	2.602(1)	Mo(4)–Br(11)	2.516(1)
Mo(2)–Br(2)	2.609(1)	Mo(4)–Br(12)	2.534(1)
Mo(2)–Br(5)	2.563(1)	Mo(4)–O(1)	2.070(5)
Mo(2)–Br(6)	2.559(1)		

Angles

Mo(2)–Mo(1)–Mo(3)	60.73(3)	Br(3)–Mo(3)–Br(5)	172.84(5)
Mo(2)–Mo(1)–Mo(4)	61.02(3)	Br(3)–Mo(3)–Br(9)	90.03(5)
Mo(3)–Mo(1)–Mo(4)	97.41(4)	Br(3)–Mo(3)–Br(10)	94.59(5)
Br(1)–Mo(1)–Br(2)	85.31(4)	Br(3)–Mo(3)–O(1)	86.2(2)
Br(1)–Mo(1)–Br(3)	91.00(4)	Br(5)–Mo(3)–Br(9)	89.45(5)
Br(1)–Mo(1)–Br(4)	176.03(4)	Br(5)–Mo(3)–Br(10)	92.56(5)
Br(1)–Mo(1)–Br(7)	89.72(5)	Br(5)–Mo(3)–O(1)	86.7(2)
Br(1)–Mo(1)–O(1)	96.7(2)	Br(9)–Mo(3)–Br(10)	90.42(4)
Br(2)–Mo(1)–Br(3)	175.82(5)	Br(9)–Mo(3)–O(1)	84.6(2)
Br(2)–Mo(1)–Br(4)	91.32(4)	Br(10)–Mo(3)–O(1)	175.0(2)
Br(2)–Mo(1)–Br(7)	88.64(4)	Mo(1)–Mo(4)–Mo(2)	58.14(3)
Br(2)–Mo(1)–O(1)	96.8(1)	Br(2)–Mo(4)–Br(4)	91.25(5)
Br(3)–Mo(1)–Br(4)	92.30(4)	Br(2)–Mo(4)–Br(6)	90.88(4)
Br(3)–Mo(1)–Br(7)	89.39(5)	Br(2)–Mo(4)–Br(11)	176.96(4)
Br(3)–Mo(1)–O(1)	85.6(1)	Br(2)–Mo(4)–Br(12)	87.10(4)
Br(4)–Mo(1)–Br(7)	88.11(5)	Br(2)–Mo(4)–O(1)	98.0(2)
Br(4)–Mo(1)–O(1)	85.7(2)	Br(4)–Mo(4)–Br(6)	171.91(4)
Br(7)–Mo(1)–O(1)	171.9(2)	Br(4)–Mo(4)–Br(11)	88.88(4)
Mo(1)–Mo(2)–Mo(3)	61.20(3)	Br(4)–Mo(4)–Br(12)	93.93(5)
Mo(1)–Mo(2)–Mo(4)	60.84(3)	Br(4)–Mo(4)–O(1)	86.1(2)
Mo(3)–Mo(2)–Mo(4)	97.59(3)	Br(6)–Mo(4)–Br(11)	89.42(5)
Br(1)–Mo(2)–Br(2)	85.41(4)	Br(6)–Mo(4)–Br(12)	93.97(5)
Br(1)–Mo(2)–Br(5)	91.21(4)	Br(6)–Mo(4)–O(1)	85.9(2)
Br(1)–Mo(2)–Br(6)	175.91(4)	Br(11)–Mo(4)–Br(12)	89.87(4)
Br(1)–Mo(2)–Br(8)	88.94(4)	Br(11)–Mo(4)–O(1)	85.0(2)
Br(1)–Mo(2)–O(1)	96.9(2)	Br(12)–Mo(4)–O(1)	174.9(2)
Br(2)–Mo(2)–Br(5)	175.83(4)	Mo(1)–Br(1)–Mo(2)	59.80(3)
Br(2)–Mo(2)–Br(6)	90.95(4)	Mo(1)–Br(1)–Mo(3)	61.69(3)
Br(2)–Mo(2)–Br(8)	88.91(4)	Mo(2)–Br(1)–Mo(3)	61.38(3)
Br(2)–Mo(2)–O(1)	97.1(2)	Mo(1)–Br(2)–Mo(2)	59.53(3)
Br(5)–Mo(2)–Br(6)	92.34(5)	Mo(1)–Br(2)–Mo(4)	61.45(3)
Br(5)–Mo(2)–Br(8)	88.57(5)	Mo(2)–Br(2)–Mo(4)	61.64(3)
Br(5)–Mo(2)–O(1)	85.8(2)	Mo(1)–Br(3)–Mo(3)	63.09(4)
Br(6)–Mo(2)–Br(8)	89.12(5)	Mo(1)–Br(4)–Mo(4)	62.70(4)
Br(6)–Mo(2)–O(1)	85.4(2)	Mo(2)–Br(5)–Mo(4)	62.64(4)
Br(8)–Mo(2)–O(1)	172.0(2)	Mo(2)–Br(6)–Mo(4)	62.81(4)
Mo(1)–Mo(3)–Mo(2)	58.06(3)	Mo(1)–O(1)–Mo(2)	76.1(2)
Br(1)–Mo(3)–Br(3)	90.11(5)	Mo(1)–O(1)–Mo(3)	80.2(2)
Br(1)–Mo(3)–Br(5)	90.67(4)	Mo(1)–O(1)–Mo(4)	79.4(2)
Br(1)–Mo(3)–Br(9)	177.90(5)	Mo(2)–O(1)–Mo(3)	79.9(2)
Br(1)–Mo(3)–Br(10)	87.48(4)	Mo(2)–O(1)–Mo(4)	79.7(2)
Br(1)–Mo(3)–O(1)	97.5(2)	Mo(3)–O(1)–Mo(4)	153.9(3)

[a] Numbers in parentheses are estimated standard deviations in the least significant digit.

The molecular orbitals calculated by the Fenske–Hall method for $[Mo_4OCl_{12}]^{2-}$ are listed in Table IV. Shown in the table are the MO energies, percentage characters of the two types of molybdenum atom and the different types of ligands in each orbital, and contributions of the $[Mo_4]^{12+}$ core MOs to the orbitals in $[Mo_4OCl_{12}]^{2-}$. There are 12 orbitals between the $1a_1$ and $5b_2$ orbitals that have been omitted from Table IV. These MOs represent the 3s lone pairs of the Cl atoms and are irrelevant to our discussion. The lowest four MOs in the table all contribute to the bonding between the metal cluster and the μ_4-O atom. The molecular orbitals above the $7a_1$ orbital and below the $16b_2$ orbital describe the Mo–Cl bonding or the 3p lone pairs of the chlorine

Table IV. Fenske–Hall Molecular Orbitals for $[Mo_4OCl_{12}]^{2-}$ [a]

level	E, eV	% Mo$_h$	Mo$_w$	Cl$_c$	Cl$_b$	Cl$_t$	O	$[Mo_4]^{12+}$ [b]
14b$_1$	1.0	65	9	4	4	5	13	7% 1b$_1$, 29% 2b$_1$, 23% 3b$_1$, 12% 4b$_1$
13b$_1$	0.6	7	76	2	4	8	4	27% 2b$_1$, 12% 3b$_1$, 20% 4b$_1$, 18% 5b$_1$
10a$_2$	−0.4	0	77	2	11	10	0	56% 2a$_2$, 5% 3a$_2$, 13% 4a$_2$
20a$_1$	−2.9	48	17	5	10	15	5	3% 2a$_1$, 51% 3a$_1$, 5% 7a$_1$
12b$_1$	−3.3	34	23	2	16	23	2	40% 1b$_1$, 12% 3b$_1$
9a$_2$	−3.9	19	19	0	7	55	0	30% 1a$_2$, 5% 3a$_2$
16b$_2$	−4.0	16	9	3	2	68	2	16% 1b$_2$, 7% 2b$_2$
19a$_1$	−4.1	41	2	3	3	46	5	9% 1a$_1$, 20% 2a$_1$, 10% 5a$_1$
15b$_2$	−4.7	2	2	1	0	95	0	
18a$_1$	−4.7	2	0	0	0	98	0	
8a$_2$	−4.9	0	2	1	9	88	0	
11b$_1$	−5.0	0	4	0	13	82	0	
7a$_2$	−5.3	0	3	1	12	84	0	
14b$_2$	−5.4	0	3	5	3	88	1	
17a$_1$	−5.4	1	6	3	3	81	6	
10b$_1$	−5.5	6	4	1	6	82	1	3% 1b$_1$
9b$_1$	−5.7	3	3	4	1	86	3	4% 1b$_1$
13b$_2$	−6.3	7	10	3	19	60	1	5% 1b$_2$, 4% 6b$_2$
16a$_1$	−6.3	22	6	0	8	64	0	4% 2a$_1$, 4% 3a$_1$, 15% 5a$_1$
12b$_2$	−6.4	1	13	3	2	81	0	8% 5b$_2$
15a$_1$	−6.6	7	9	1	4	74	5	5% 1a$_1$, 7% 9a$_1$
14a$_1$	−6.7	10	13	8	0	68	1	13% 2a$_1$, 4% 8a$_1$
6a$_2$	−6.8	21	22	0	11	46	0	25% 1a$_2$, 12% 2a$_2$, 6% 3a$_2$
8b$_1$	−6.9	13	3	0	14	67	3	4% 3b$_1$, 8% 6b$_1$
13a$_1$	−7.2	12	8	0	0	79	1	5% 6a$_1$, 12% 7a$_1$
11b$_2$	−7.3	11	24	6	11	45	2	13% 1b$_2$, 11% 2b$_2$, 7% 4b$_2$
10b$_2$	−8.2	9	7	1	74	9	0	5% 1b$_2$, 3% 2b$_2$, 6% 5b$_2$
5a$_2$	−8.3	2	11	11	69	7	0	8% 4a$_2$
12a$_1$	−8.5	4	1	8	80	4	3	4% 5b$_1$
7b$_1$	−8.4	7	4	14	64	11	0	
9b$_2$	−8.6	7	1	31	55	5	1	
4a$_2$	−8.7	7	6	13	70	4	0	6% 1a$_2$, 3% 3a$_2$, 4% 5a$_2$
6b$_1$	−8.7	12	4	16	54	7	6	4% 1b$_1$, 9% 3b$_1$
11a$_1$	−9.0	6	2	13	73	5	0	
5b$_1$	−9.5	10	5	11	66	6	2	10% 4b$_1$, 4% 5b$_1$
8b$_2$	−9.9	4	16	61	14	5	0	4% 1b$_2$, 3% 2b$_2$, 7% 4b$_2$, 4% 5b$_2$
3a$_2$	−10.0	8	14	15	59	3	0	9% 1a$_2$, 4% 2a$_2$, 7% 3a$_2$
7b$_2$	−10.5	6	20	4	69	1	0	12% 2b$_2$, 7% 3b$_2$, 3% 4b$_2$
10a$_1$	−10.6	8	15	11	59	1	6	10% 3a$_1$, 8% 4a$_1$
2a$_2$	−11.0	22	8	45	23	1	0	17% 1a$_2$, 10% 2a$_2$
9a$_1$	−11.2	15	12	61	8	3	1	13% 2a$_1$, 7% 4a$_1$
4b$_1$	−11.5	17	14	37	26	1	5	18% 1b$_1$, 10% 2b$_1$
8a$_1$	−11.6	23	3	59	12	0	3	7% 2a$_1$, 13% 3a$_1$
6b$_2$	−11.7	25	9	54	11	1	0	29% 1b$_2$
7a$_1$	−12.2	18	15	4	5	6	52	27% 1a$_1$, 3% 4a$_1$
3b$_1$	−12.3	18	16	3	9	1	53	13% 1b$_1$, 20% 2b$_1$
5b$_2$	−13.1	7	26	0	0	3	63	6% 2b$_2$, 16% 3b$_2$
1a$_1$	−28.6	4	8	0	0	0	88	5% 1a$_1$, 5% 2a$_1$

[a] The HOMO and the LUMO are the 10a$_2$ and 13b$_1$ orbitals, respectively. [b] Contributions less than 3% are not included.

atoms. The remaining six highest-occupied orbitals thus may be considered to account for the metal–metal bonding in the compound as we shall see later, although considerable metal–ligand mixing does occur. The HOMO for $[Mo_4OCl_{12}]^{2-}$ is the 10a$_2$ orbital and it is localized on the wingtip molybdenum atoms. The LUMO, the 13b$_1$ orbital, is also metal-based and mainly localized in the wingtips. An Xα–SW calculation gave a HOMO and a LUMO of the same nature with a energy gap of 0.3 eV. The results calculated for the $[Mo_4OBr_{12}]^{2-}$ compound are very similar to those for $[Mo_4OCl_{12}]^{2-}$, except that the HOMO–LUMO gap given by the Xα–SW calculation is only 0.12 eV in this case.

There is a close similarity between the $[Mo_4OCl_{12}]^{2-}$ ion and a previously studied butterfly cluster $Mo_4(OH)_8Cl_4$.[9] The only qualitative structural difference between the two systems is the μ_4-O atom. However, the interaction of the μ_4-O atom with the metal atoms has a significant effect on the metal–metal bonding in $[Mo_4OCl_{12}]^{2-}$ compared with $Mo_4(OH)_8Cl_4$, whereas the bonding between the chlorine atoms and the metal cluster is not greatly affected by the oxygen atom. It is therefore reasonable

Table V. Mulliken Populations of the Canonical Orbitals of $[Mo_4]^{12+}$ for $[Mo_4O]^{10+}$ and $[Mo_4OCl_{12}]^{2-}$

orbital	$[Mo_4]^{12+}$	$[Mo_4O]^{10+}$	$[Mo_4OCl_{12}]^{2-}$
1a$_1$	2.00	1.03	1.15
1b$_2$	2.00	1.99	1.61
2a$_1$	2.00	1.55	1.40
1b$_1$	2.00	1.89	1.75
1a$_2$	2.00	2.00	1.87
2b$_2$	2.00	1.93	1.10
3a$_1$	0.00	1.91	1.83
2b$_1$	0.00	0.67	0.71
2a$_2$	0.00	0.00	1.74
4a$_1$	0.00	0.16	0.61
3b$_2$	0.00	0.48	0.67
4b$_2$	0.00	0.05	0.50
5a$_1$	0.00	0.00	0.67
3b$_1$	0.00	0.01	0.66
3a$_2$	0.00	0.00	0.70
4b$_1$	0.00	0.01	0.34
6a$_1$	0.00	0.07	0.29
4a$_2$	0.00	0.00	0.53
5b$_2$	0.00	0.00	0.54
7a$_1$	0.00	0.00	0.46
5b$_1$	0.00	0.00	0.24

that we first look at the metal–(μ_4-O) bonding interaction and, then concentrate mainly on the metal–metal bonding in the cluster compound since metal–chlorine bonding of this type has already been studied in a great detail.[9]

The way in which the μ_4-O atom interacts with the metal cluster in $[Mo_4OCl_{12}]^{2-}$ can be seen in Table IV where the lowest four molecular orbitals account for practically all of the bonding between the oxygen atom and the Mo_4 core. No other filled orbitals have any significant contribution from the oxygen atom. The lowest orbital, 1a$_1$, has very little Mo contribution and is predominantly the 2s atomic orbital of the oxygen atom as might be expected. The strong Mo–O bonding character in the 5b$_2$, 3b$_1$ and 7a$_1$ orbitals can be attributed to overlap of the 3b$_2$, 2b$_1$, and 1a$_1$ orbitals of the $[Mo_4]^{12+}$ core with the oxygen 2p$_y$, 2p$_x$ and 2p$_z$ orbitals, respectively. In fact the 3b$_2$, 2b$_1$ and 1a$_1$ orbitals of the $[Mo_4]^{12+}$ core make practically no contribution to any other occupied MOs in $[Mo_4OCl_{12}]^{2-}$. It is therefore convenient to consider first the bonding in an intermediate cluster, $[Mo_4O]^{10+}$, and then look at the interaction of this intermediate with other ligands in the system.

Such a description of the bonding is also supported by the Mulliken population analyses as shown in Table V. Listed in Table V are the Mulliken populations of the canonical orbitals of the metal cluster core first in $[Mo_4]^{12+}$ itself, and then in $[Mo_4O]^{10+}$ and $[Mo_4OCl_{12}]^{2-}$. It can be seen from the table that due to strong Mo–O interaction the population in the 1a$_1$ orbital of the cluster core is substantially reduced from $[Mo_4]^{12+}$ to $[Mo_4O]^{10+}$, and the unoccupied 2b$_1$ and 3b$_2$ orbitals become significantly populated. In addition, the 3a$_1$ orbital is also almost fully populated in $[Mo_4O]^{10+}$, which can be attributed to charge transfer out of the 1a$_1$ orbital as a result of the Mo–O interaction. Thus, the 1a$_1$ orbital as well as the 2b$_1$ and 3b$_2$ orbitals of $[Mo_4]^{12+}$ may all be regarded as acceptors of charge from the oxygen atom in $[Mo_4O]^{10+}$. It is important to note that the populations of these $[Mo_4]^{12+}$ orbitals in $[Mo_4O]^{10+}$ remain essentially unchanged in $[Mo_4OCl_{12}]^{2-}$, which means that they are dominated by the oxygen atom.

To illustrate the bonding character of the μ_4-O atom to the metal atoms, we present in Figure 2 the contour plots of the 1a$_1$ and 7a$_1$ orbitals of $[Mo_4OCl_{12}]^{2-}$. It may be mentioned that our calculation shows a reversed order of the 2b$_2$ and 3a$_1$ orbitals in the $[Mo_4]^{12+}$ core compared to the previous results[9] for $Mo_4(OH)_8Cl_4$. This may be attributed to the different basis functions employed for the molybdenum atom as well as to the different nuclear geometry for $[Mo_4]^{12+}$ in our calculations, and is not important.

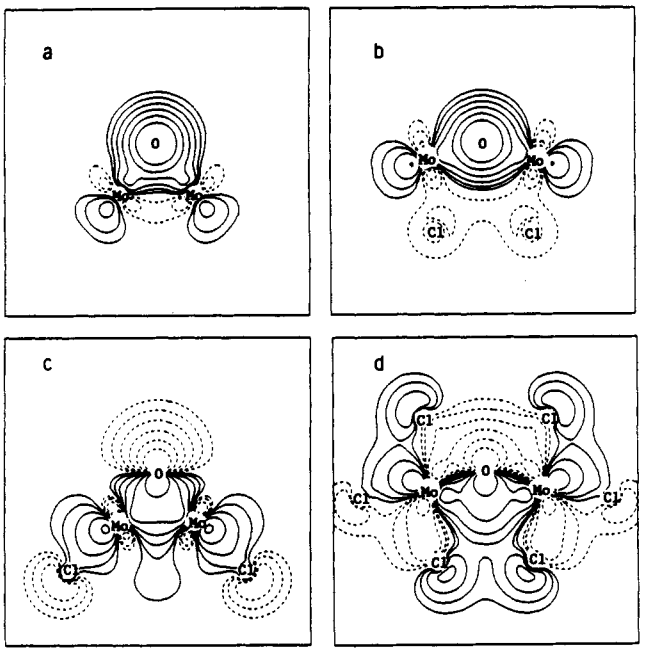

Figure 2. Contour plots of (a) the $1a_1$ orbital in a plane containing two hinge molybdenum atoms and the oxygen atom, (b) the $1a_1$ orbital in a plane containing two wingtip molybdenum atoms and the oxygen atom, (c) the $7a_1$ orbital in a plane as for (a), and (d) the $7a_1$ orbital in a plane as for (b) for $[Mo_4OCl_{12}]^{2-}$. Dashed lines indicate negative contour values. Contour values used in all plots are as the follows: 0.005, 0.01, 0.02, 0.04, 0.08, and 0.16.

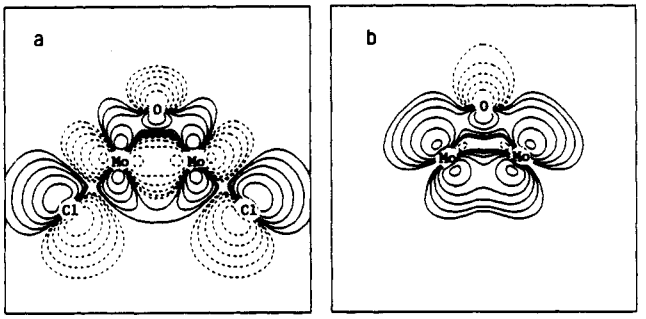

Figure 3. Contour plots of (a) the $19a_1$ orbital and (b) the $20a_1$ orbital both in a plane containing two hinge molybdenum atoms and the oxygen atom for $[Mo_4OCl_{12}]^{2-}$.

We turn now to discussion of the metal–metal cluster bonding in $[Mo_4OCl_{12}]^{2-}$. As seen in Table IV, the six highest occupied orbitals may be regarded as accommodating the 12 cluster electrons in $[Mo_4OCl_{12}]^{2-}$. Among the six orbitals, the lower five, namely, the $16b_2$, $19a_1$, $9a_2$, $12b_1$, and $20a_1$ orbitals, are all metal–metal bonding either between the hinge molybdenum atoms or between the hinge and the wingtip atoms. These orbitals are mainly correlated with the $1b_2$, $2a_1$, $1a_2$, $1b_1$, and $3a_1$ orbitals of the $[Mo_4]^{12+}$ cluster core. It should be noted from Table IV that metal–metal bonding character may be distributed over two or more orbitals of the same symmetry as a result of metal–ligand mixing. For example, the $6a_2$ and $9a_2$ orbitals, and the $11b_2$ and $16b_2$ orbitals are pairs that jointly contribute to the Mo_h–Mo_w bonding. The $10a_2$ orbital, the HOMO for $[Mo_4OCl_{12}]^{2-}$, is localized on the wingtips, and should be regarded as nonbonding in nature because of the large separation between the wingtips and the oxygen atom in between. Shown in Figure 3a,b are contour plots of the $19a_1$ and $20a_1$ orbitals, respectively, as illustrations of the metal–metal bonding in $[Mo_4OCl_{12}]^{2-}$. The contours were plotted on a plane containing the hinge molybdenum atoms and the μ_4-O atom, and illustrate clearly the bonding character between the metal atoms.

The $10a_2$ orbital has a dominant contribution from the $2a_2$ orbital of $[Mo_4]^{12+}$ as shown in Table IV. This can also be seen

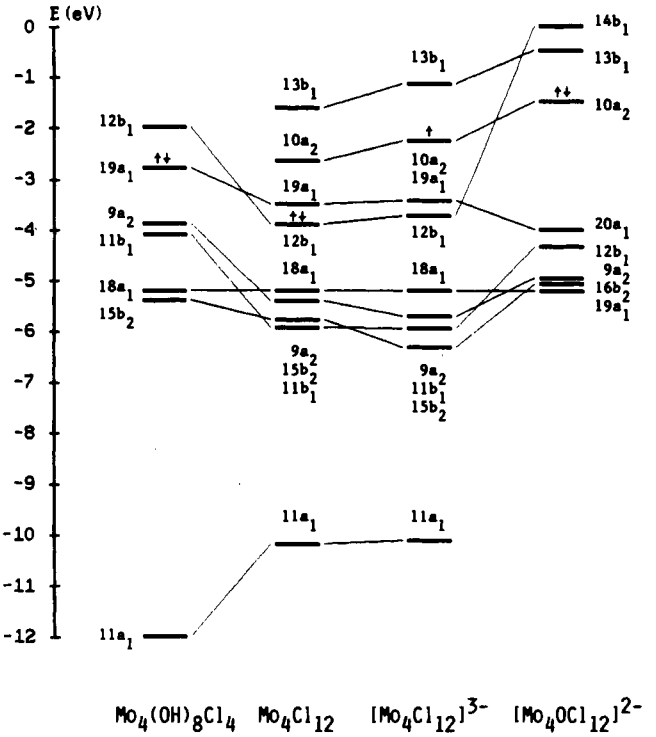

Figure 4. Correlation diagram comparing the molecular orbitals for metal–metal interaction in the butterfly cluster compounds. The arrows indicate the HOMO in each compound. In $Mo_4(OH)_8Cl_4$, the $12b_1$ orbital was added with its energy 0.8 eV higher than the $19a_1$ orbital.

in Table V where the empty $2a_2$ orbital in $[Mo_4]^{12+}$ has become highly populated (1.73) in $[Mo_4OCl_{12}]^{2-}$. The electrons in the $2a_2$ orbital may be regarded as transferred from the occupied $2b_2$ orbital in $[Mo_4]^{12+}$ which, while not affected by the μ_4-O atom, is directed toward the incoming Cl atoms.

The metal cluster bonding in $[Mo_4OCl_{12}]^{2-}$ may be compared with that in other butterfly compounds of similar structure but without a μ_4-O atom, namely, the 12-electron compounds, $Mo_4(OH)_8Cl_4$[9] and Mo_4Cl_{12}, and the 15-electron compound,[7] $[Mo_4Cl_{12}]^{3-}$. Comparison and correlation of the orbitals that are primarily involved in the metal-metal interactions in these compounds are shown in Figure 4, where the results of the Fenske–Hall molecular orbital calculations are used. The orbital energies in the figure for each compound have been shifted in such a way that the $18a_1$ orbitals in the first three columns and the $19a_1$ orbital in the last column match with each other. These orbitals are all primarily responsible for σ bonding between the hinge molybdenum atoms although there is some π-antibonding interaction with the attached terminal Cl atoms (see Figure 3a).

It has been shown[9] that the occupied molecular orbitals listed in the first column of Figure 4 for $Mo_4(OH)_8Cl_4$ are all primarily involved in the metal–metal cluster bonding. These orbitals correlate essentially to the first five orbitals plus the $3a_1$ orbital of the $[Mo_4]^{12+}$ core as listed in Table V. The bonding character of each of them has been illustrated clearly in the previous study of this compound.[9] The HOMO and the LUMO in $Mo_4(OH)_8Cl_4$ are the $19a_1$ and $12b_1$ orbitals, respectively. The two orbitals are both primarily localized in the hinge molybdenum atoms and may be regarded as bonding and antibonding counterparts for the hinge atoms. Orbitals of similar character also occur for Mo_4Cl_{12} (the second column of Figure 4), but the order of the $19a_1$ and $12b_1$ orbitals is now reversed. Thus the HOMO in Mo_4Cl_{12} is the $12b_1$ orbital, a result obtained also by the Xα–SW calculation. For $[Mo_4Cl_{12}]^{3-}$, the additional three electrons occupy the $19a_1$ and $10a_2$ orbitals that are empty in Mo_4Cl_{12}. As a matter of fact, the presence of the three additional electrons causes no significant differences between the orbital diagrams for Mo_4Cl_{12} and $[Mo_4Cl_{12}]^{3-}$, as shown in Figure 4. The HOMO in

$[Mo_4Cl_{12}]^{3-}$ correlates with the HOMO in $[Mo_4OCl_{12}]^{2-}$, both being the $10a_2$ orbitals, which are essentially nonbonding and localized on the wingtips. The LUMO in $[Mo_4Cl_{12}]^{3-}$ is the $13b_1$ orbital. In the chloride-supported cluster compounds, both $12b_1$ and $13b_1$ orbitals are antibonding between the hinges and bonding between the wingtips in a similar way, but the $12b_1$ orbital has some bonding character between the hinge and the wingtip, while the $13b_1$ orbital is antibonding in this respect.

As indicated in Figure 4, bonding of the μ_4-O atom to the metal cluster has significant effects on the bonding within the metal cluster in $[Mo_4OCl_{12}]^{2-}$ as compared to the cases in the cluster compounds without the oxygen atom. First of all, there is no orbital of a_1 symmetry in $[Mo_4OCl_{12}]^{2-}$ that correlates with the lowest metal–metal bonding orbital, the $11a_1$ orbital, in the compounds without the μ_4-O atom. The $11a_1$ orbital in these compounds is correlated to the $1a_1$ orbital of the $[Mo_4]^{12+}$ core as indicated earlier. In $[Mo_4OCl_{12}]^{2-}$, however, the $1a_1$ orbital has been shown to be involved exclusively in the bonding interaction with the μ_4-O atom, and thus does not contribute to the metal–metal bonding. Also, because of the metal–oxygen interaction, the $14b_1$ orbital that is correlated to the $12b_1$ orbital in the first three columns in Figure 4 has been pushed up in accord with its metal–oxygen antibonding character (see also Table IV), which leaves the $10a_2$ orbital as the HOMO in $[Mo_4OCl_{12}]^{2-}$. By noting the correlation between the lowest five orbitals (from $19a_1$ to $20a_1$) of $[Mo_4OCl_{12}]^{2-}$ and the highest five occupied orbitals (from $15b_2$ to $19a_1$) of $Mo_4(OH)_8Cl_4$ in Figure 4, it may be said that, effectively, the interaction of a $(\mu_4\text{-}O)^{2-}$ ion with the metal cluster has pumped out two electrons from the lowest metal–metal bonding $11a_1$ orbital in the latter to the $10a_2$ orbital of high energy in the former that has a nonbonding character between the metal atoms on the wingtips. As a result, the direct metal–metal cluster bonding in the actual compound $[Mo_4OBr_{12}]^{2-}$ would be weaker than that in $Mo_4(O\text{-}i\text{-}Pr)_8Br_4$[6] which has been modeled by $Mo_4(OH)_8Cl_4$ with all 12 cluster electrons entering metal–metal bonding orbitals. But this by no means suggests that $[Mo_4OBr_{12}]^{2-}$ is not as stable as $Mo_4(O\text{-}i\text{-}Pr)_8Br_4$. As a matter of fact, the $[Mo_4OBr_{12}]^{2-}$ compound should be greatly stabilized by the strong bonding interaction between the metal cluster and the μ_4-O atom.

The metal–metal bonding schemes as shown in Figure 4 also offer an interesting comparison of the metal–metal distances in the actual compounds. While in $Mo_4(O\text{-}i\text{-}Pr)_8Br_4$ the Mo_h–Mo_h distance is shorter than the Mo_h–Mo_w distance,[6] the situation is just the opposite in $[Mo_4Cl_{12}]^{3-}$.[3] This may be attributed to the cancellation of the bonding effect in the $19a_1$ orbital by the occupation of the $12b_1$ orbital that is antibonding between the hinge atoms. For $[Mo_4OBr_{12}]^{2-}$, however, the bond length ratio is the same as that in $Mo_4(O\text{-}i\text{-}Pr)_8Br_4$. This is because loss of the metal–metal bonding effect of the $11a_1$ orbital which is absent in $[Mo_4OBr_{12}]^{2-}$ but present in $Mo_4(O\text{-}i\text{-}Pr)_8Br_4$ should affect both types of metal–metal distances about equally, since the $11a_1$ orbital is delocalized over all metal atoms.

The results of the present Xα–SW calculation also suggest that the energy difference between the HOMO and the LUMO in $[Mo_4OBr_{12}]^{2-}$ may be very small, namely, 0.12 eV. This feature of the electronic structure raises two interesting questions. One concerns whether a second-order Jahn–Teller effect that might occur because of the small HOMO–LUMO energy gap and the symmetries of the HOMO ($10a_2$) and the LUMO ($13b_1$) in $[Mo_4OBr_{12}]^{2-}$ (see also Table IV). The second concerns the magnetic properties. We deal with the possible Jahn–Teller effect first. The direct product of the a_2 and b_1 symmetry species of the HOMO and LUMO belongs to the b_2 irreducible representation, which is just the symmetry of one of the six vibrational normal modes of the Mo_4 butterfly unit in C_{2v} symmetry. Therefore, a second-order Jahn–Teller distortion is formally possible and would take the form of the b_2 normal vibration in $[Mo_4OBr_{12}]^{2-}$. However, as indicated clearly by the structural data of the compound, no such distortion actually occurs. A closer look at the electronic structure of the compound, as given by the Xα–SW calculation, shows that the HOMO and the LUMO in $[Mo_4OBr_{12}]^{2-}$ are both dominated by the wingtip atoms, namely, 75% for the HOMO and 77% for the LUMO, with remaining contributions mainly from the terminal bromine atoms. If the distortion were to occur, the symmetry of the compound would be lowered so that only one plane of symmetry could remain and the HOMO and the LUMO would be mixed because of the symmetries of the orbitals both being a″ in that case. In general the driving force for second-order Jahn–Teller distortion is a mixing of the HOMO and the LUMO that leads to forming a new bond or to bond-strengthening effects in the system with a stabilization of the HOMO and a destabilization of the LUMO. As a result, the whole system would be stabilized by the distortion. In the case of $[Mo_4OBr_{12}]^{2-}$, however, the mixing of the HOMO and the LUMO will not significantly enhance any bonding effects that could further stabilize the system because of the very nature of the orbitals.

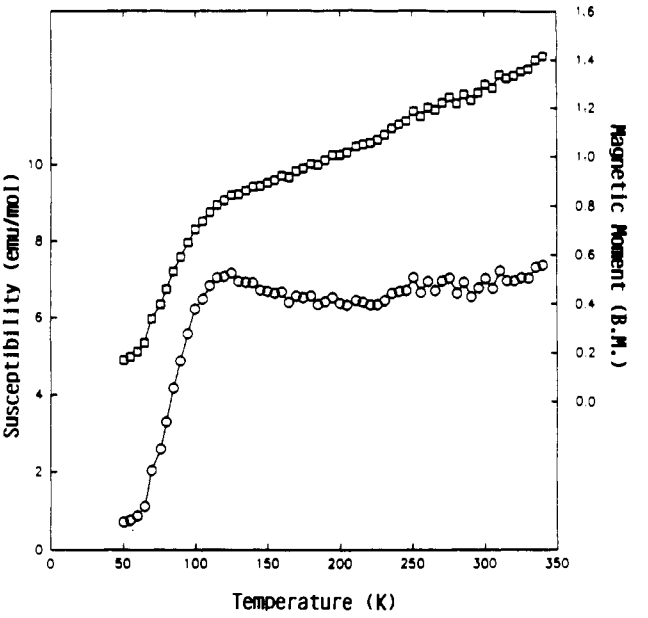

Figure 5. Magnetic susceptibility ($\times 10^{-4}$ and cycles) and magnetic moment (squares) vs temperature for $[Bu_4N]_2[Mo_4OBr_{12}]$.

We turn now to the question of how the small HOMO–LUMO gap influences the magnetic properties of the system. Figure 5 shows a plot of χ_m^{corr} and the magnetic moment $\mu = 2.83(\chi_m T)^{1/2}$ vs temperature. In a qualitative sense, these results are consistant with a Boltzmann equilibrium between a diamagnetic ground state and one or more thermally accessible paramagnetic excited states. It has been found impossible to fit the data to a simple singlet–triplet manifold (i.e., to use a Bleaney–Bowers equation). We are inclined to believe that this is because one or more additional paramagnetic states, besides the lowest-lying triplet, are also thermally accessible at the higher temperatures of measurement. However, we have not attempted to achieve a parameterized fitting since this would not provide any useful information.

Acknowledgment. We are grateful to the National Science Foundation for financial support. We also thank Prof. T. Datta for the magnetic susceptibility data.

Supplementary Material Available: Tables of crystallographic data, bond lengths, bond angles, and anisotropic displacement parameters and ORTEP drawings of cations, the interstitial molecule, and unit cell contents for compound **1** (14 pages). Ordering information is given on any current masthead page.